*LETTER* Communicated by Bard Ermentrout

# A-Type $K^+$ Current Can Act as a Trigger for Bursting in the Absence of a Slow Variable

**Natalia Toporikova**
*ntoporik@ math.fsu.edu*
*Department of Mathematics, Florida State University, Tallahassee, FL 32306, U.S.A.*

**Joël Tabak**
*joel@neuro.fsu.edu*
**Marc E. Freeman**
*freeman@neuro.fsu.edu*
*Department of Biological Science, Florida State University, Tallahassee, FL 32306, U.S.A.*

**Richard Bertram**
*bertram@math.fsu.edu*
*Department of Mathematics, Florida State University, Tallahassee, FL 32306, U.S.A.*

**Models of bursting in single cells typically include two subsystems with different timescales. Variations in one or more slow variables switch the system between a silent and a spiking state. We have developed a model for bursting in the pituitary lactotroph that does not include any slow variable. The model incorporates fast, noninactivating calcium and potassium currents (the spike-generating mechanism), as well as the fast, inactivating A-type potassium current ($I_A$). $I_A$ is active only briefly at the beginning of a burst, but this brief impulse of $I_A$ acts as a burst trigger, injecting the spike trajectory close to an unstable steady state. The spiraling of the trajectory away from the steady state produces a period of low-amplitude spiking typical of lactotrophs. Increasing the conductance of A-type potassium current brings the trajectory closer to the unstable steady state, increasing burst duration. However, this also increases interburst interval, and for larger conductance values, all activity stops. To our knowledge, this is the first example of a physiologically based, single-compartmental model of bursting with no slow subsystem.**

## 1 Introduction

Bursting, a common pattern of electrical activity in excitable cells, is characterized by brief periods of fast spiking (the active phase) and quiescent

 © 2008 Massachusetts Institute of Technology

periods (the silent phase). The bursting pattern is usually associated with a higher level of hormone or neurotransmitter secretion (Cazalis, Dayanithi, & Nordmann, 1985; Nunemaker, Straume, DeFazio, & Moenter, 2003; Stojilkovic, Zemkova, & Van Goor, 2005) when compared with continous spiking patterns. There is evidence that bursting may have important roles in signaling in neurons (Gabbiani, Metzner, Wessel, & Koch, 1996; Lisman, 1997).

Numerous mathematical models of bursting in neural and endocrine cells have been developed (Coombes & Bressloff, 2005). Typically the model can be split into fast and slow subsystems, and bursting oscillations are driven by slow activity-dependent oscillations in the slow variables. The fast subsystem is usually bistable, with a stable steady state coexisting with a stable periodic (spiking) solution. One or more slow variables then switch the system between these attractors (Rinzel, 1985, 1987). The duration of the burst depends on the dynamics of the slow variable(s).

In a recent mathematical model of the pituitary lactotroph, we demonstrated that adding a fast A-type $K^+$ current can increase secretion (Tabak, Toporikova, Freeman, & Bertram, 2007). This is in spite of the fact that $I_A$ is a hyperpolarizing current and would typically be expected to reduce secretion by hyperpolarizing the membrane. The stimulatory action occurs by converting the spiking pattern to bursting. Surprisingly, we found cases of bursting in which bistability was not present in the fast subsystem. Also, bursting persisted when the only slow variable in the model, the intracellular $Ca^{2+}$ concentration, was held fixed. Figure 1 illustrates the difference between this type of bursting and standard bursting based on bistability and a slow variable. In both panels, slow oscillations of $Ca^{2+}$ occur in parallel with the slow voltage oscillations. Nevertheless, $Ca^{2+}$ plays a different role in each case. In Figure 1A , bursting is terminated if intracellular $Ca^{2+}$ is held constant. This is classic bursting, where the slow changes in $Ca^{2+}$ are driving the bursts. In contrast, for the case shown in Figure 1B, clamping $Ca^{2+}$ does not stop the bursts. This indicates that $Ca^{2+}$ is not driving the bursts but simply follows them. The goal of this work is to analyze the latter type of bursting and contrast its mechanism with the standard bursting mechanisms.

To facilitate the analysis, we removed nonessential elements from the lactotroph model. The slow variable in the original model ($Ca^{2+}$ concentration) is removed, and the original $Ca^{2+}$-activated $K^+$ current is treated as a constant conductance current. This results in a simplified model with only three variables, all of which vary on a fast timescale relative to the burst period. We show that bursting can be produced with this model in the absence of a slow variable and analyze the dynamic mechanism for this novel form of bursting.

## 2 Model

The model is a simplification of a recent model for the electrical activity of the pituitary lactotroph (Tabak et al., 2007). The simplified model

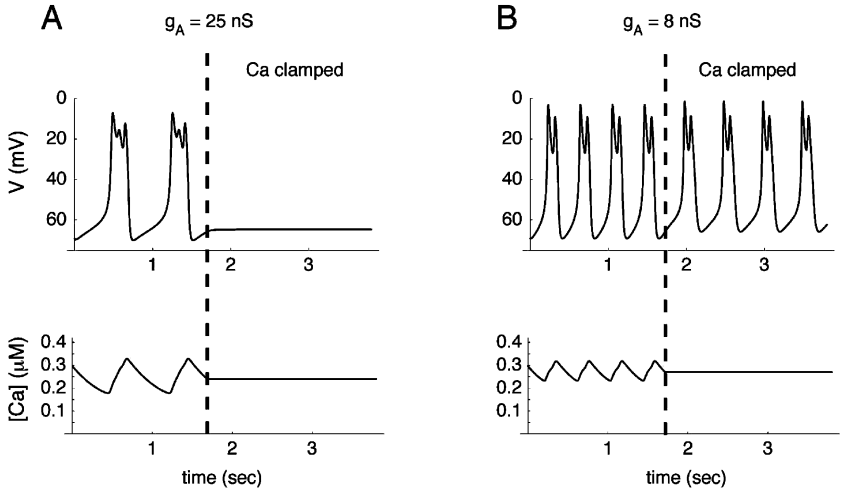


Figure 1: Bursting in a lactotroph model with different A-type current conductances (Tabak et al., 2007). (A) For $g_A = 25$ nS, bursting is terminated if intracellular $Ca^{2+}$ is held constant. The bursting mechanism relies on slow variations of $Ca^{2+}$. (B) For $g_A = 8$ nS, clamping $Ca^{2+}$ does not stop the bursts. This indicates an intrinsic bursting mechanism independent of $Ca^{2+}$.

incorporates three voltage-gated currents: a $Ca^{2+}$ current ($I_{Ca}$), a delayed rectifier $K^+$ current ($I_{DR}$), and a fast and transient A-type $K^+$current ($I_A$). There is also a non-voltage-gated leak current $I_L$. The dynamics of the three variables $V$ (membrane potential), $n$ (activation of $I_{DR}$), and $e$ (inactivation of $I_A$) are described by:

$$C\frac{dV}{dt} = -(I_{Ca} + I_{DR} + I_A + I_L) \tag{2.1}$$

$$\tau_n \frac{dn}{dt} = n_\infty(V) - n \tag{2.2}$$

$$\tau_e \frac{de}{dt} = e_\infty(V) - e. \tag{2.3}$$

The ionic currents are given by

$$I_{Ca} = g_{Ca} m_\infty (V - V_{Ca}) \tag{2.4}$$

$$I_{DR} = g_{DR} n (V - V_K) \tag{2.5}$$

$$I_A = g_A a_\infty e (V - V_K) \tag{2.6}$$

$$I_L = g_L (V - V_K), \tag{2.7}$$

Table 1: Parameter Values.

| Parameter | Value | Definition |
|---|---|---|
| $C$ | 10 pF | Membrane capacitance |
| $g_{Ca}$ | 2 nS | Maximal conductance of $Ca^{2+}$ channels |
| $V_{Ca}$ | 50 mV | Reversal potential for $Ca^{2+}$ |
| $v_m$ | −20 mV | Voltage value at midpoint of $m_\infty$ |
| $s_m$ | 12 mV | Slope parameter of $m_\infty$ |
| $g_{DR}$ | 4.4 nS | Maximal conductance of DR $K^+$ channels |
| $V_K$ | −75 mV | Reversal potential for $K^+$ |
| $v_n$ | −5 mV | Voltage value at midpoint of $n_\infty$ |
| $s_n$ | 10 mV | Slope parameter of $n_\infty$ |
| $\tau_n$ | 43 ms | Time constant of $n$ |
| $g_A$ | 0–20 nS | Maximal conductance of A channels |
| $v_a$ | −20 mV | Voltage value at midpoint of $a_\infty$ |
| $s_a$ | 10 mV | Slope parameter of $a_\infty$ |
| $v_e$ | −60 mV | Voltage value at midpoint of $e_\infty$ |
| $s_e$ | 5 mV | Slope parameter of $e_\infty$ |
| $g_L$ | 0.3 nS | Maximal conductance of leak current |
| $\tau_e$ | 20 ms | Time constant of $e$ |

and the steady-state activation functions have the form

$$x_\infty = \frac{1}{1+\exp\left(\frac{V_x - V}{s_x}\right)}, \tag{2.8}$$

where $x$ represents an activation variable ($m, n$, and $a$). The inactivation steady-state function is

$$e_\infty = \frac{1}{1+\exp\left(\frac{V - V_e}{s_e}\right)}\,. \tag{2.9}$$

When $I_A$ is not present ($g_A = 0$), the model has the form of the Morris-Lecar model (Morris & Lecar, 1981).

Parameter values are given in Table 1. Values of the kinetic parameters for $I_{Ca}$ were obtained from Lledo, Legendre, Israel, and Vincent (1990), and the values for $I_{DR}$ and $I_A$ are based on Herrington and Lingle (1994). Equations were integrated, and bifurcation diagrams were constructed, using the software package XPPAUT (Ermentrout, 2002). The fourth-order Runge-Kutta integration method was used, with a time step of 0.5 ms. Reducing the time step had no effect on the simulations. The code for this model is freely available online at www.math.fsu.edu/bertram/software/pituitary.

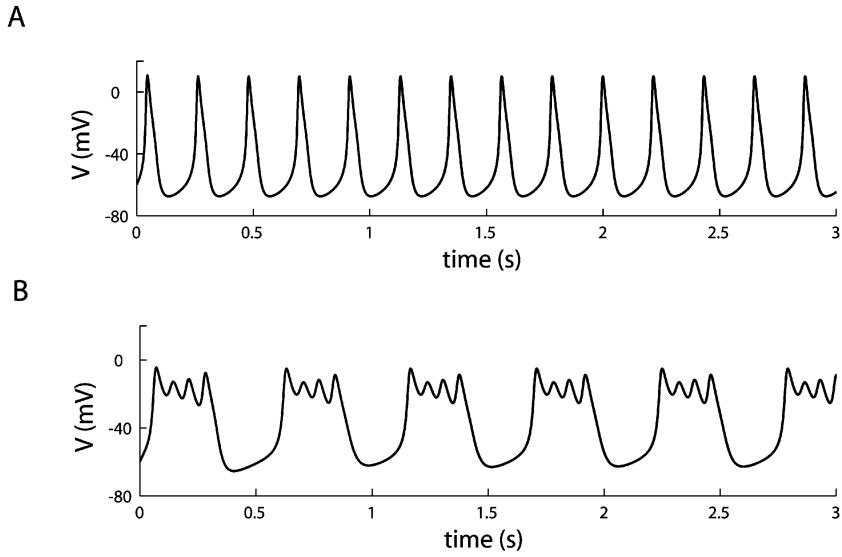


Figure 2: $I_A$ converts spiking to bursting. (A) For $g_A = 0$ nS, the model cell is spiking. (B) Increasing the A-type $K^+$ channel conductance to $g_A = 13$ nS converts spiking to bursting.

## 3 Results

**3.1 $I_A$ Converts Spiking into Bursting.** In our recent model of the pituitary lactotroph we found that adding a small amount of A-type $K^+$ current converts the model cell from a spiker to a burster (Tabak et al., 2007). Figure 2 illustrates the effect of increasing $g_A$ from 0 to 13 nS in the reduced lactotroph model. For $g_A = 0$ (see Figure 2A), the model cell is spiking. When $g_A$ is increased to 13 nS (see Figure 2B), the spiking is converted into bursting. The duration of the burst, approximately 600 ms, is much larger than the time constants of all model variables ($\tau_n = 43$ ms, $\tau_e = 20$ ms and the membrane time constant is 33 ms).

Rush and Rinzel (1995) also obtained a switch to bursting by adding an A current to a spiking model. In their case, though, the inactivation variable of the A current acted as a slow variable, switching the fast subsystem between a high (oscillatory) state and a low, stable state. To demonstrate that this is not the case in our model, we plot in Figure 3 the bifurcation diagram of the $V$-$n$ subsystem with $e$ treated as a parameter. For $e = 0$, the system has a single unstable steady state surrounded by a stable limit cycle. As $e$ is increased, the steady state becomes stable through a subcritical Hopf bifurcation (HB). The periodic branch born at the Hopf bifurcation emerges as unstable but gains stability at a saddle node of periodics (SNP)

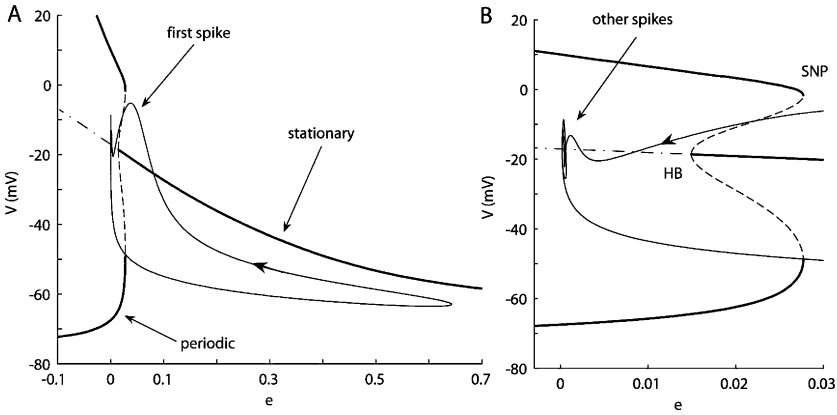


Figure 3: (A) Bifurcation diagram of the $V$-$n$ subsystem with inactivation variable $e$ treated as a parameter ($g_A = 13$ nS). Thick lines represent stable solutions, and thin lines represent unstable ones. The maximum and minimum of the periodic solution are shown as upper and lower periodic branches, respectively. The projection of the burst trajectory of the full system is superimposed, and does not follow the bifurcation diagram of the V-n subsystem. (B) The same for the smaller range of $e$. Most of the active phase of the burst occurs near $e = 0$. HB: Hopf bifurcation. SNP: saddle node periodic bifurcation.

bifurcation. Between the HB and SNP bifurcations is a region of bistability, with coexisting stable steady state and periodic solutions. However, the burst trajectory (superimposed) does not utilize this bistability region, and indeed does not follow the bifurcation diagram of the $V$-$n$ subsystem. The spikes of the active phase occur for low values of $e$, and indeed it is clear from Figure 3B that $e$ is nearly zero during the most of the active phase; therefore, variations of $e$ do not terminate the burst. Together, these observations indicate that the bursting shown in Figure 2B cannot be described using fast-slow analysis with $e$ as the slow variable.

**3.2 $I_A$ Acts as a Burst Trigger.** To investigate the mechanism of burst generation, we plot the two potassium currents of the model, $I_{DR}$ and $I_A$, during one full burst cycle. $I_{DR}$ reflects the burst trajectory. $I_A$ is near zero during most of the active phase, peaking at the onset of the burst (see Figure 4). Is the entire $I_A$ impulse necessary for bursting? To address this question, we blocked $I_A$ at different time points during the burst. In Figure 5A we blocked $I_A$ (set $g_A = 0$) after 80 ms, which is midway along the downstroke of the impulse. As a result, the burst is totally eliminated, and only a single large-amplitude spike is produced. Note also that when $I_A$ is blocked, subsequent bursts do not occur.

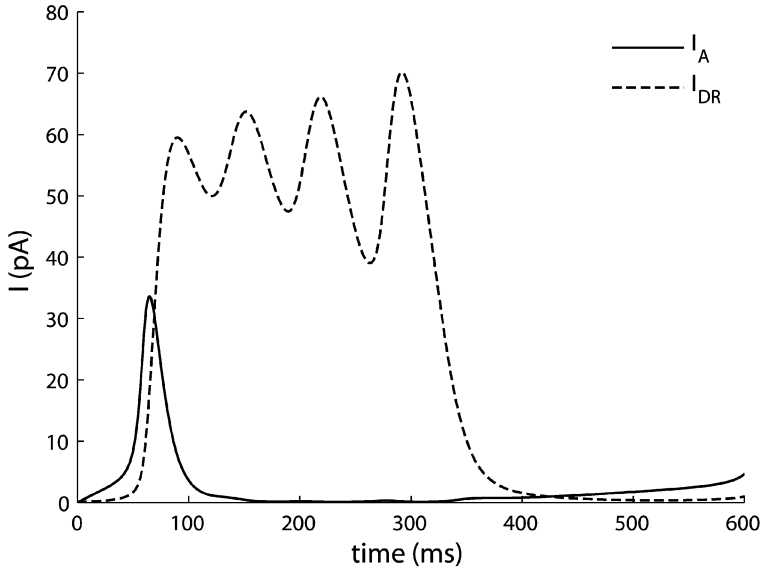


Figure 4: Two $K^+$ currents during one full burst cycle ($g_A = 13$ nS). There is an impulse in $I_A$ at the beginning of the burst, and $I_A$ is near zero during the remainder of the active phase.

Thus, a nearly complete $I_A$ impulse is necessary to induce bursting, but is it sufficient? If we block $I_A$ only 7 ms later, at 87 ms (see Figure 5B), then the burst appears, but it is short, with only 2 spikes per burst. If $I_A$ is blocked at 90 ms (see Figure 5C), when the $I_A$ impulse is almost complete, the burst is complete. That is, the burst has the same length as the control burst in Figure 4. Thus, the $I_A$ impulse alone is sufficient to induce bursting; $I_A$ can be set to zero throughout the remainder of the burst, and the burst will proceed. Therefore, the $I_A$ impulse acts as a trigger for bursting.

How does the $I_A$ impulse trigger the burst? To address this question, we view the burst trajectory in the $V$-$n$-$I_A$ space. Figures 6A to 6C correspond to the $I_A$ current profiles of Figures 5A to 5C. Figure 6D shows the trajectory without any block of $I_A$ (current profile in Figure 4).

When $g_A = 0$ the system spikes, and the spiking trajectory is in the $V$-$n$ plane, surrounding an unstable steady state. This spiking trajectory is shown in gray in Figure 6D. When $g_A = 13$ nS (see Figure 6A), the trajectory leaves the $V$-$n$ plane during the $I_A$ impulse. Blocking $I_A$ at 80 ms returns the trajectory to the $V$-$n$ plane, where it approaches the spiking limit cycle around the unstable steady state (open circle).

When $I_A$ is blocked later, at 87 ms, the trajectory reenters the $V$-$n$ plane closer to the unstable steady state and spirals around it twice before approaching the spiking limit cycle (see Figure 6B). Each spiral is a

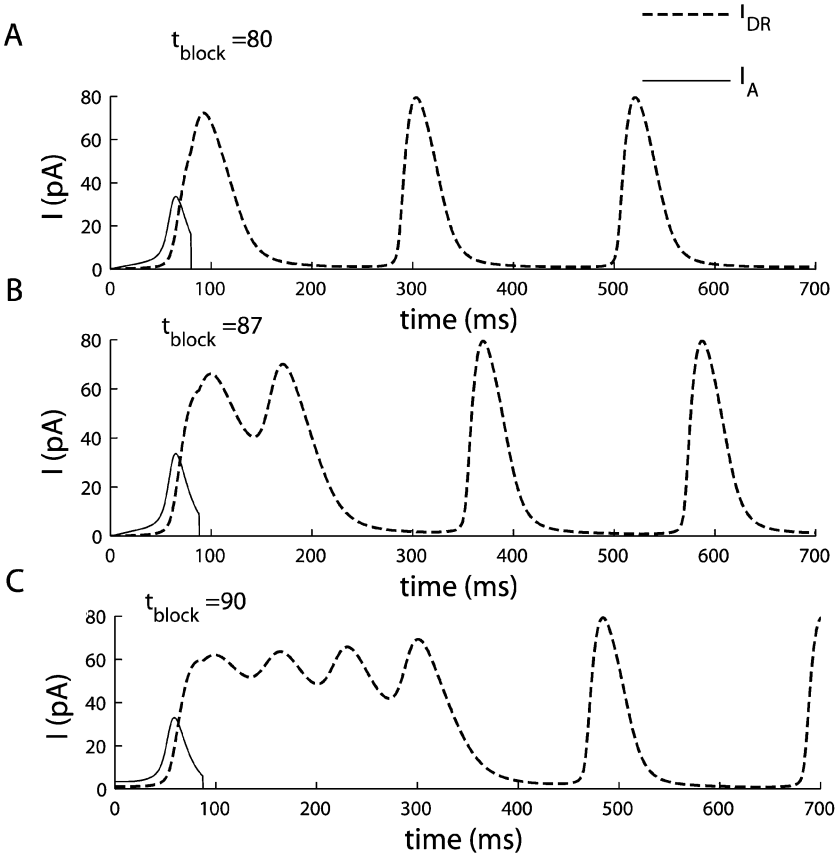


Figure 5: The effect of blocking $I_A$ at different time points. (A) $I_A$ blocked at 80 ms eliminates the burst. (B) $I_A$ blocked at 87 ms reduces the burst to two spikes. (C) $I_A$ blocked at 90 ms results in a complete burst. Before the block, $g_A = 13$ nS.

low-amplitude electrical impulse during the active phase of the burst (see Figure 5B). If $I_A$ is blocked later, at 90 ms, the trajectory reenters even closer to the unstable steady state (see Figure 6C). As a result, more spirals occur before the trajectory moves out toward the spiking limit cycle. This produces a burst with more low-amplitude spikes (see Figure 5C). When $I_A$ is not blocked, the trajectory enters the $V$-$n$ plane near the unstable steady state at the end of the $I_A$ impulse (see Figure 6D). The remainder of the burst takes place in the $V$-$n$ plane, so $I_A$ plays no role after the impulse.

**3.3 Increase in $I_A$ Increases Burst Duration.** Not only does the $I_A$ impulse trigger the burst, but its magnitude determines the burst length. In

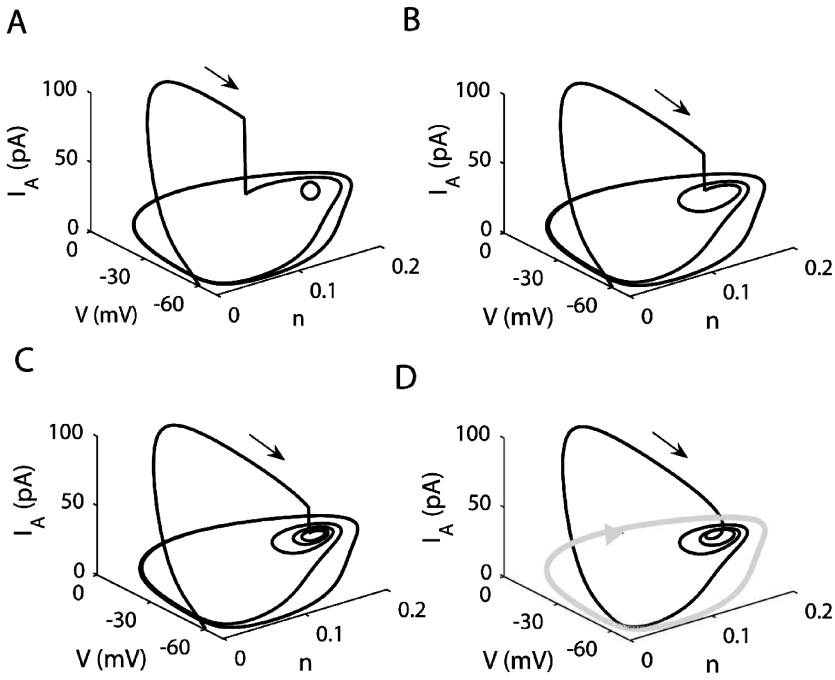


Figure 6: The effect of $I_A$ block shown in the $V$-$n$-$I_A$ space. (A) $I_A$ blocked at 80 ms. The open circle in the $V$-$n$ plane represents the unstable steady state. (B) $I_A$ blocked at 87 ms. (C) $I_A$ blocked at 90 ms. (D) Trajectory with unblocked $I_A$ ($g_A = 13$ nS). The gray curve represents the continuous spiking limit cycle ($g_A = 0$).

Figure 7A, $g_A$ is increased from 0 to 23 nS in steps. When $g_A$ is increased to 3 nS, the spiking pattern switches to a two-spike burst. Another spike is added when $g_A$ is increased to 7 nS. Increasing $g_A$ to13 nS adds a fourth spike to the burst, and so on. There are also more complex spiking patterns between the regular $n$-spike bursts. We found chaotic patterns between the two- and three-spike bursts, three- and four-spike bursts, as well as between the four- and five-spike patterns (see Figure 7C). Further increase of $g_A$ , larger than 20.85 nS, stops all activity.

Figure 7B shows the bifurcation diagram of the $V$-$e$ subsystem with $n$ treated as a parameter for different values of $g_A$. The $n$-nullcline is also shown. The lower and upper branches of the $z$-shaped bifurcation diagram consist of stable equilibria of the $V$-$e$ subsystem, while equilibria on the middle branch are unstable. For lower values of $g_A$ ($g_A = 0$ and $g_A = 7$ nS), there is a single depolarized unstable steady state of the full $V$-$e$-$n$ system. Increasing $g_A$ stretches the bifurcation diagram so that the lower

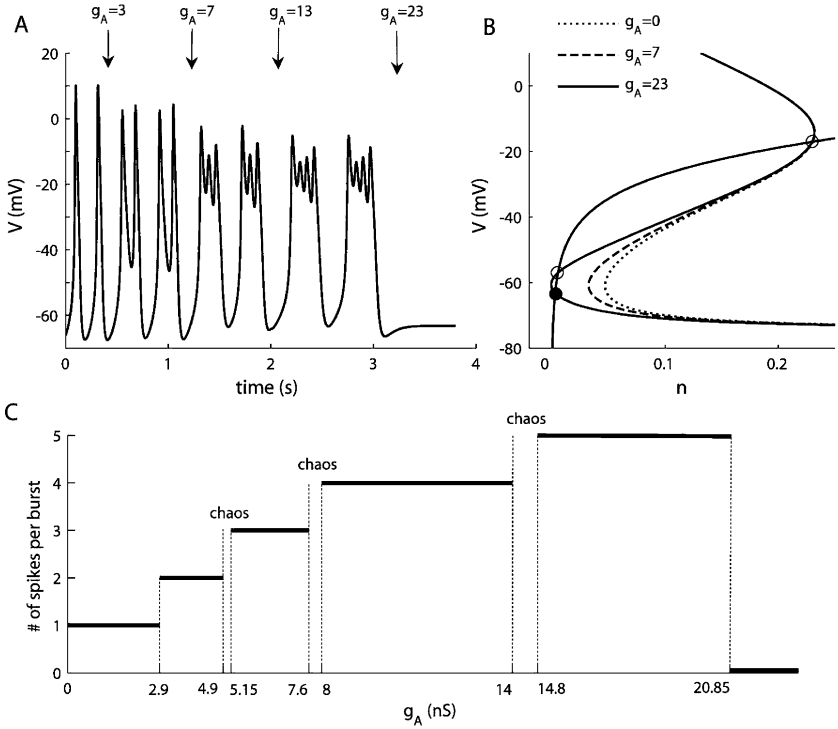


Figure 7: (A) Increasing $g_A$ increases the number of spikes per burst until activity stops. (B) Bifurcation diagram for the $V$-$e$ subsystem with $n$ treated as a parameter. $g_A = 0$ (dotted line), $g_A = 7$ nS (dashed line), and $g_A = 23$ nS (solid line). The $n$-nullcline is also shown. Open circles represent unstable steady states, and the closed circle denotes a stable steady state. (C) Number of spikes per burst as function of $g_A$. The chaotic bursting regions are between the dashed lines.

knee moves to the left. When $g_A = 23$ nS, the lower knee intersects the $n$-nullcline, and two new steady states appear, one of which is stable. The trajectory is now attracted to this lower stable steady state, and bursting stops.

To explain how the burst increases in length with an increase in $g_A$, we project the burst trajectory onto the $V$-$n$ plane. Figure 8A shows the superimposed trajectories with $g_A = 0$ and $g_A = 3$ nS. The dashed curve is the spiking trajectory when $g_A = 0$. The unstable steady state (open circle) is the intersection of the $V$ and $n$ nullclines (dot-dashed curves). When $g_A$ is increased to 3 nS (solid curve), the rapidly activating hyperpolarizing current reduces the rise in voltage during the upstroke of the spike (arrow), so the trajectory comes closer to the unstable spiral. Movement around

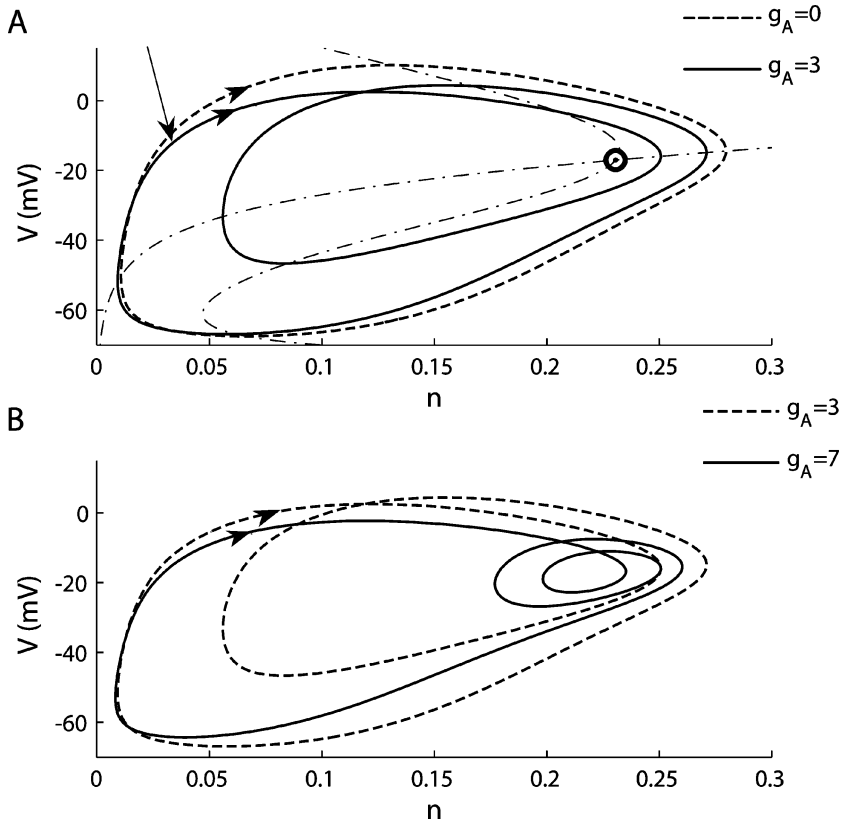


Figure 8: Mechanism by which increasing the $I_A$ impulse magnitude increases the burst duration. (A) Trajectories projected onto the $V$-$n$ plane with $g_A = 0$ nS (dashed line) and $g_A = 3$ nS (solid line). The dot-dashed lines are the $V$ and $n$ nullclines for $g_A = 0$. The arrow indicates the beginning of the spike upstroke, and the open circle is an unstable steady state. (B) The $V$-$n$ phase plane for $g_A = 3$ nS (dashed line) and $g_A = 7$ nS (solid line). The increase in $g_A$ moves the trajectory closer to the unstable steady state, producing more spikes per burst.

this spiral produces a burst with two spikes. For larger $I_A$ ($g_A = 7$ nS), the trajectory has a closer approach to the unstable spiral (see Figure 8B), making three turns around it before entering the silent phase of the burst. Thus, a larger $I_A$ moves the trajectory closer to the unstable spiral, creating a longer active phase of the burst. Note that the number of revolutions around the unstable spiral is highly sensitive to the way that the trajectory approaches the spiral at the beginning of the burst. Thus, chaotic spiking patterns can be produced, as mentioned above.

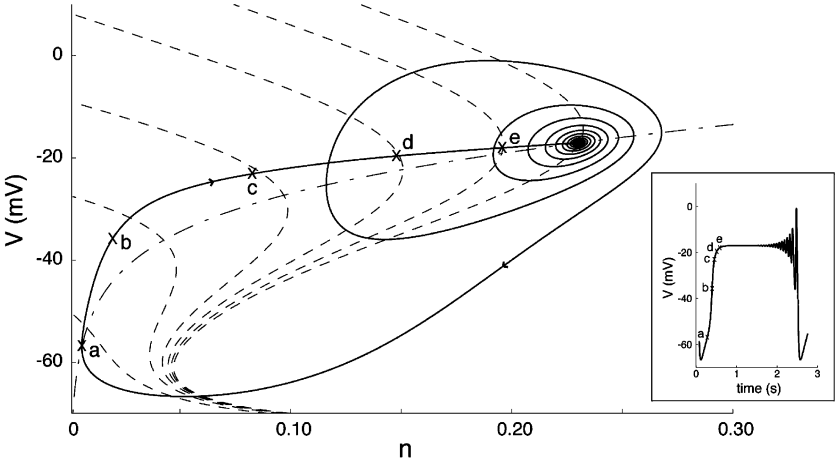


Figure 9: Bending of the trajectory in $V$-$n$ space for $\tau_e = 80$ ms. Points a–e correspond to values of $e$ of 0.5, 0.2, 0.1, 0.05, and 0.02. For each of these points, the corresponding $V$-nullcline of the $V$-$n$ subsystem is represented (dashed z-shaped curve), as is the $n$-nullcline (dot-dashed). As $V$ increases, $e$ decreases, moving the $V$-nullcline upward and to the right. The intersections of the $n$-nullcline and the $V$-nullclines corresponding to points a–e are steady states of the $V$-$n$ subsystem, not of the $V$-$n$-$e$ system. Only the intersection for $e = 0$ defines a steady state of the full system. Inset: Time course of membrane potential during one "burst." Most of the burst period is spent in the active phase where $e \approx 0$.

**3.4 How Is the Trajectory Driven Toward an Unstable Steady State?** The previous results show that by turning on at the beginning of a burst, $I_A$ pushes the trajectory toward the unstable steady state of the $V$-$n$ subsystem. For larger $I_A$, the trajectory passes closer to that unstable steady state. How can $I_A$ bring the trajectory so close to a repellent state? As shown in Figure 3, the steady state of the $V$-$n$ subsystem becomes stable when $e$ increases above its value at the Hopf bifurcation ($\sim$0.02). At the beginning of a burst, before $I_A$ is fully inactivated, this stable steady state can behave as an attractor and thus bend the trajectory as shown above, before becoming unstable as $e$ reaches 0.

This is shown in Figure 9. Although $e$ is not a slow variable, we have slowed it ($\tau_e$ increased fourfold to 80 ms) to better demonstrate the effect, as Drover, Rubin, Su, & Ermentrout (2004) did. The figure shows the trajectory of the system projected in the $V$-$n$ plane. Five points (a–e) along the trajectory at the onset of a burst are represented. They correspond to values of $e$ of 0.5, 0.2, 0.1, 0.05, and 0.02. For each of these points, the corresponding $V$-nullcline of the $V$-$n$ subsystem is shown (z-shaped, dashed). The intersection of each $V$-nullcline and the $n$-nullcline (dot-dashed curve)

is a stable steady state of the $V$-$n$ subsystem for the corresponding $e$ and a pseudo steady state for the full system. Thus, if $e$ were frozen when the trajectory is at point a, it would be attracted to the stable steady state just above a. However $e$ decreases, so the z-shaped curve moves up and to the right, and so does the attracting steady state. The trajectory thus never reaches any of the pseudo steady states, but it is bent while tracking these moving targets. When $e$ is near zero, the steady state becomes unstable, but only weakly so. Thus, the trajectory spirals away, but slowly. A similar situation occurs when $e$ is not slowed, but then the z-shaped curves move faster, so the trajectory is less affected and does not come as close to the unstable steady state as $I_A$ fully inactivates.

Figure 9 illustrates the fundamental difference between standard bursting (i.e., square wave bursting) and the bursting presented here. In standard bursting, a slow variable slowly takes the system to transition points where activity abruptly switches between high (oscillatory) and low (stationary) states. In our model, a fast variable quickly moves the only steady state of the $V$-$n$ subsystem between a high, unstable position to a series of low, stable positions, thus creating the different phases of the burst.

Finally, this highlights the two characteristics of $I_A$ needed to produce this type of bursting. First, $I_A$ needs to activate quickly, so that the unstable steady state of the $V$-$n$ subsystem can become attracting. Second, it needs to inactivate; otherwise, the system would remain indefinitely in that steady state.

## 4 Discussion

We have shown a new mechanism for bursting in a simplified excitable cell model. In classical bursters, the system can be split into fast and slow subsystems, and bursting oscillations are driven by slow activity-dependent oscillations in the slow variables. The fast subsystem is usually bistable, with a stable steady state coexisting with a stable periodic (spiking) solution. One or more slow variables then switch the system between these attractors. Unlike classical bursting, the bursting that we describe is produced without a slow variable. An A-type $K^+$ current converts the spiking pattern to bursting by injecting the trajectory to a location near an unstable spiral. Motion around the spiral creates low-amplitude spikes riding on a voltage plateau, similar to what is observed in pituitary lactotrophs (Oxford & Tse, 1993; Van Goor, Zivadinovic, Martinez-Fuentes, & Stojilkovic, 2001), somatotrophs (Van Goor, Li, & Stojilkovic, 2001), corticotrophs (Kuryshev, Childs, & Ritchie, 1996; Kuryshev, Haak, Childs, & Ritchie, 1997), and clonal pituitary cells (Adler et al., 1983). $I_A$ also plays its traditional role of slowing the next occurrence of an impulse, contributing to the silent phase duration between the bursts.

The A-type potassium current is widely known to delay spiking or reduce firing frequency (Connor, Walter, & McKown, 1977). It has been shown

that changes in this current's conductance and dynamic properties can result in bursting (Rush & Rinzel, 1995). However, in the Rush-Rinzel model, the A-current inactivation acts as a slow variable to terminate the burst. This is a classic fast-slow system, with the $I_A$ inactivation variable accumulating during the burst. The hyperpolarization following each spike decreases the inactivation of $I_A$ until the current becomes large enough to terminate the burst. Thus, increasing $g_A$ decreases the burst duration. In our model, $I_A$ does not terminate the burst since it quickly inactivates and no deinactivation occurs during the burst since the model cell stays depolarized until the end of the burst. Also, in our model, increasing $g_A$ increases the burst duration, although if $g_A$ is too large, the bursting is terminated altogether, and the model cell becomes silent. Thus, the transition sequence from tonic spiking to bursting to quiescence as $g_A$ is increased in our model differs from the sequence in the square-wave burster of Rush and Rinzel.

Another example of bursting driven by a slowly inactivated $K^+$ current is a model of pyramidal cells in the electrosensory lateral lobe of weakly electric fish (Doiron, Laing, Longtin, & Maler, 2002). This is a two-compartment model, with impulse propagation between the soma and an active dendrite. Like the Rush and Rinzel model, this "ghostbuster" model has two timescales. The single slow variable is the $K^+$ current inactivation in the dendrite, which accumulates during the burst. The soma begins to spike, and the spike is transmitted to the dendrite and back again to the soma. As this Ping-Pong effect continues, the $K^+$ current in the dendrite inactivates. This speeds up the spiking, so that eventually the soma spikes so fast that the dendrite cannot keep up. The lack of a dendritic spike then terminates the burst. Thus, in contrast to the model of Rush and Rinzel, it is the accumulation of inactivation, not deinactivation, that terminates the bursting. In our model, however, there is no slowly accumulating process.

The A-type $K^+$ current has been used in a wide variety of excitable cell models (Connor, Walter, & McKown, 1977; Gerber & Jakobsson, 1993; Rybak, Paton, & Schwaber, 1997; Wustenberg et al., 2004). However, there are no examples of $I_A$ inducing bursting of the nature described here. Why does this happen in our model? The physiological set of parameters used in the lactotroph model puts the unstable steady state at a depolarized value. This is just below the upper branch of the z-shaped bifurcation diagram (see Figure 7B). Had the intersection been on the upper branch, the steady state would have been stable. Thus, the unstable steady state is only weakly repelling, so that the trajectory spirals several times before leaving the neighborhood of the steady state. If the steady state had occurred lower on the bifurcation diagram (e.g., by shifting $I_{DR}$ activation to lower $V$), the steady state would be more repelling, and it would require more $I_A$ current to bend the trajectory toward the steady state. Bursting could be recovered by decreasing the time constant of $I_{DR}$ activation, which would make the steady state less repelling. Also, increasing the efficiency of $I_A$ by slowing its inactivation variable or increasing its conductance would help bring the

trajectory toward the unstable steady state. However, note that increasing $g_A$ could create a stable hyperpolarized steady state (see Figure 7B) of the full *V-n-e* system, so the steepness of the activation function of $I_A$ would need to be increased. Thus, bursting is robust to parameter changes, but others may not have observed this type of $I_A$-induced bursting because of the location of the unstable steady state or the time-dependent properties of the $I_A$ and $I_{DR}$ currents used in their models. To our knowledge, this is the first example of bursting without a slow variable in a single-compartment, physiologically based cell model.

## Acknowledgments

This work was supported by the National Institute of Drug Abuse Grant no. DA-19356 to R.B. and M.E.F.

## References

Adler, M., Wong, B. S., Sabol, S. L., Busis, N., Jackson, M. B., & Weight, F. F. (1983). Action potentials and membrane ion channels in clonal anterior pituitary cells. *Proc. Natl. Acad. Sci. U.S.A, 80*(7), 2086–2090.

Cazalis, M., Dayanithi, G., & Nordmann, J. J. (1985). The role of patterned burst and interburst interval on the excitation-coupling mechanism in the isolated rat neural lobe. *J. Physiol., 369*, 45–60.

Connor, J. A., Walter, D., & McKown, R. (1977). Neural repetitive firing: Modifications of the Hodgkin-Huxley axon suggested by experimental results from crustacean axons. *Biophys. J., 18*(1), 81–102.

Coombes, S., & Bressloff, P. C. (2005). *Bursting: The genesis of rhythm in the nervous system.* Singapore: World Scientific.

Doiron, B., Laing, C., Longtin, A., & Maler, L. (2002). Ghostbursting: A novel neuronal burst mechanism. *J. Comput. Neurosci., 12*(1), 5–25.

Drover, J., Rubin, J., Su, J. H., & Ermentrout, B. (2004). Analysis of a canard mechanism by which excitatory synaptic coupling can synchronize neurons at low firing frequencies. *SIAM J. Appl. Math., 65*, 69–92.

Ermentrout, B. (2002). *Simulating, analyzing, and animating dynamical systems: A guide to Xppaut for researchers and students*. Philadelphia: SIAM.

Gabbiani, F., Metzner, W., Wessel, R., & Koch, C. (1996). From stimulus encoding to feature extraction in weakly electric fish. *Nature, 384* (6609), 564–567.

Gerber, B., & Jakobsson, E. (1993). Functional significance of the A-current. *Biol. Cybern., 70*(2), 109–114.

Herrington, J., & Lingle, C. J. (1994). Multiple components of voltage-dependent potassium current in normal rat anterior pituitary cells. *J. Neurophysiol., 72*(2), 719–729.

Kuryshev, Y. A., Childs, G. V., & Ritchie, A. K. (1996). Corticotropin-releasing hormone stimulates Ca2+ entry through L- and P-type Ca2+ channels in rat corticotropes. *Endocrinology, 137*(6), 2269–2277.

Kuryshev, Y. A., Haak, L., Childs, G. V., & Ritchie, A. K. (1997). Corticotropin releasing hormone inhibits an inwardly rectifying potassium current in rat corticotropes. *J. Physiol, 502*(Pt. 2) 265–279.

Lisman, J. E. (1997). Bursts as a unit of neural information: Making unreliable synapses reliable. *Trends Neurosci., 20*(1), 38–43.

Lledo, P. M., Legendre, P., Israel, J. M., & Vincent, J. D. (1990). Dopamine inhibits two characterized voltage-dependent calcium currents in identified rat lactotroph cells. *Endocrinology, 127*(3), 990–1001.

Morris, C., & Lecar, H. (1981). Voltage oscillations in the barnacle giant muscle fiber. *Biophys J., 35*(1), 193–213.

Nunemaker, C. S., Straume, M., DeFazio, R. A., & Moenter, S. M. (2003). Gonadotropin-releasing hormone neurons generate interacting rhythms in multiple time domains. *Endocrinology, 144*(3), 823–831.

Oxford, G. S., & Tse, A. (1993). Modulation of ion channels underlying excitation-secretion coupling in identified lactotrophs and gonadotrophs. *Biol. Reprod., 48*(1), 1–7.

Rinzel, J. (1985). Bursting oscillations in an excitable membrane model. In B. Sleeman & D. Jones (Eds.), *Ordinary and partial differential equations.* New York: Springer-Verlag.

Rinzel, J. (1987). A formal classification of bursting mechanisms in excitable systems. In E. Teramoto & M. Yamaguti (Eds.), *Mathematical topics in population biology, morphogenesis, and neurosciences* (pp. 267–281). Berlin: Springer-Verlag.

Rush, M. E., & Rinzel, J. (1995). The potassium A-current, low firing rates and rebound excitation in Hodgkin-Huxley models. *Bull. Math. Biol., 57*(6), 899–929.

Rybak, I. A., Paton, J. F., & Schwaber, J. S. (1997). Modeling neural mechanisms for genesis of respiratory rhythm and pattern. I. Models of respiratory neurons. *J. Neurophysiol., 77*(4), 1994–2006.

Stojilkovic, S. S., Zemkova, H., & Van Goor, F. (2005). Biophysical basis of pituitary cell type–specific Ca2+ signaling-secretion coupling. *Trends in Endocrinology and Metabolism, 16*(4), 152–159.

Tabak, J., Toporikova, N., Freeman, M., & Bertram, R. (2007). Low dose of dopamine may stimulate prolactin secretion by increasing fast potassium currents. *J. Comput. Neurosci., 22*(2), 211–222.

Van Goor, F., Li, Y. X., & Stojilkovic, S. S. (2001). Paradoxical role of large-conductance calcium-activated K+ (BK) channels in controlling action potential-driven Ca2+ entry in anterior pituitary cells. *J. Neurosci., 21*(16), 5902–5915.

Van Goor, F., Zivadinovic, D., Martinez-Fuentes, A. J., & Stojilkovic, S. S. (2001). Dependence of pituitary hormone secretion on the pattern of spontaneous voltage-gated calcium influx: Cell type–specific action potential secretion coupling. *J. Biol. Chem., 276*, 33840–33846.

Wustenberg, D. G., Boytcheva, M., Grunewald, B., Byrne, J. H., Menzel, R., & Baxter, D. A. (2004). Current- and voltage-clamp recordings and computer simulations of Kenyon cells in the honeybee. *J. Neurophysiol., 92*(4), 2589–2603.

Received August 21, 2006; accepted January 24, 2007.